Available online at www.sciencedirect.com
SCIENCE DIRECT
ELSEVIER
Icarus 174 (2005) 90–104
ICARUS
www.elsevier.com/locate/icarus

The Meudon Multicolor Survey (2MS) of Centaurs and trans-neptunian objects: extended dataset and status on the correlations reported

A. Doressoundiram [a,*], N. Peixinho [a,b], C. Doucet [c], O. Mousis [d], M.A. Barucci [a], J.M. Petit [d], C. Veillet [e]

[a] *LESIA, Observatoire de Paris, UMR CNRS 8109, F-92195 Meudon Principal cedex, France*
[b] *Centro de Astronomia e Astrofisica da Universidade de Lisboa, PT-1349-018 Lisboa, Portugal*
[c] *DSM/DAPNIA/SAP, CEA-Saclay, 91191 Gif-sur-Yvette cedex, France*
[d] *Observatoire de Besançon, B.P. 1615, 25010 Besançon cedex, France*
[e] *Canada–France–Hawaii Telescope Corporation, PO Box 1597, Kamuela, HI 96743, USA*

Received 28 November 2003; revised 16 September 2004

Abstract

We present here the latest $B-V$, $V-R$, and $R-I$ color measurements obtained with the CFH12K mosaic camera of the 3.6-m Canada–France–Hawaii Telescope (CFHT). This work is the latest extension of the Meudon Multicolor Survey (2MS) and extends the total number of Centaurs and trans-neptunian objects (TNOs) in the dataset to 71. With this large and homogeneous dataset, we performed relevant statistical analyses to search for correlations with physical and orbital parameters and interrelations with related populations (cometary nuclei and irregular satellites). With a larger dataset, we confirm the correlations found for the Classical TNOs in our previous survey: some colors are significantly correlated with perihelion distance and inclination. The only exception is with the eccentricity. However, results strongly depend on which objects are considered Classicals, and with a dynamically more restricted definition these correlations are no longer present. We also find that strongly significant trends with orbital parameters are not detected for Centaurs, Plutinos or scattered disk objects (SDOs). We also make for the first time reliable statistical comparison between TNOs and related populations (e.g., Centaurs, irregular satellites, short period comets—i.e., SPCs). We find that (1) the colors of SPCs do not match either their TNO or Centaur precursors, and this suggests that some process modifies the surface of SPCs at entry into the inner Solar System. The only exception concerns colors of SDOs from which we could statistically assess that SPCs and SDOs could be drawn from a same single parent distribution. (2) Not surprisingly, Centaurs are compatible with each of the Edgeworth–Kuiper belt dynamical groups at a highly significant level except with the SDOs. (3) Centaurs' colors still present a strong dichotomy between a neutral/slightly red group (e.g., Chiron) and a very red group (e.g., Pholus). (4) The irregular satellite population is not compatible with any of the Centaur, Plutino or Classical populations; however, the similarity of their color properties with SDOs suggests that both groups can be extracted from the same parent distribution. However, due to the small number of Centaurs and SDOs these conclusions cannot be taken as definitive.

Keywords: Trans-neptunian objects; Kuiper belt objects; Centaurs; Photometry

1. Introduction

Beyond the orbit of Neptune exists a population of bodies remaining from the formation of the Solar System. These are the Kuiper belt or trans-neptunian objects (TNOs). Scientific interest in these bodies arises because this region of the Solar System may preserve some of the most primitive materials available to direct investigation. With the large and

* Corresponding author.
E-mail address: alain.doressoundiram@obspm.fr (A. Doressoundiram).

0019-1035/$ – see front matter
doi:10.1016/j.icarus.2004.09.009

high quality color datasets available, strong and significant results have been found. For a complete review on the photometric surveys, their results and the related references, see Doressoundiram (2003). We will just summarize here the main results.

One of the most puzzling features of the Kuiper belt, which has been confirmed by numerous surveys (e.g., Tegler and Romanishin, 2000; Boehnhardt et al., 2001; Doressoundiram et al., 2002; Trujillo and Brown, 2002; Peixinho et al., 2004), is the optical color diversity that seems to prevail among the observed TNOs. TNOs and Centaurs have surfaces showing a wide range of colors and spectral reflectance, from neutral to very red. Moreover, observational surveys revealed the existence of a group of Classical TNOs with very red colors in dynamically 'cold' orbits beyond about 40 AU from the Sun (Tegler and Romanishin, 2000). This color diversity seems also to extend to near infrared wavelengths, although relatively few visible-NIR color datasets are available (see McBride et al., 2003, and references therein). The strong color anisotropy found is important because it is diagnostic of some physical effects processing the surfaces of TNOs and/or some possible composition diversity.

Correlations between colors and orbital parameters have also been identified. Statistical analyses point to correlations between optical colors and some orbital parameters (i, e, q) for the classical Kuiper belt. (e.g., Hainaut and Delsanti, 2002; Trujillo and Brown, 2002; Peixinho et al., 2004). In contrast, no clear trends are obvious for Plutinos, scattered objects or Centaurs. Another important result is the absence of correlation of colors with size or heliocentric distance for any of the populations of outer Solar System objects. It should be noted that some correlations appear weaker with increasing datasets, especially with HST and 8–10-m class telescopes (see Doressoundiram, 2003; Stephens et al., 2003).

We have started since 1997 an intensive photometric survey, the Meudon Multicolor Survey (2MS) with the aim of collecting a large and homogeneous (same observational strategy and data reduction procedure) set of color data for TNO and Centaur objects. With this large dataset obtained mostly at CFHT, we performed relevant statistical analyses to search interrelations with related populations and correlations with physical and orbital parameters. Results from these works can be found in the previous papers: Barucci et al. (1999, 2000); Doressoundiram et al. (2001, 2002).

In this paper, we present the latest extension of the 2MS, including the last data obtained at the CFHT with the CFH12K camera, now replaced by the MegaCam wide field camera. We will analyze this larger dataset and investigate whether correlations found previously are confirmed and how significant they are. We will also look for possible new trends, especially for populations poorly sampled in previous works (e.g., scattered disk objects). Finally, with this extended dataset we will compare the color distribution of TNOs with other related populations: cometary nuclei, Centaurs and irregular satellites.

2. Observations

2.1. Data acquisition

The observing runs were conducted at the Canada–France–Hawaii Telescope (CFHT) 3.6-m telescope. Observations of TNOs and Centaurs were taken during four nights in 5–7 June 2003 and 31 October 2003 under photometric conditions, dark skies and a seeing between 0.6–1.0 arcsec most of the time. These observations cover the B, V, R, and I bands, with images obtained through a photometric sequence *RVBIV* aimed at minimizing systematic errors due to object's rotation (see Doressoundiram and Boehnhardt, 2003, for details on the specific observational strategy of TNOs). The observations were performed with the CFH12K camera positioned at the prime focus of the CFHT. The camera was equipped with twelve 2048×4096 pixels back side illuminated CCDs from the MIT Lincoln Laboratories. Only one of these CCDs was employed for imaging during the observing run. The scale at the prime focus (f/4) is $0.206''$/pix and the field of view is $7' \times 14'$.

The observed objects and their observational circumstances are reported in Table 1. The telescope and instrument characteristics are described in Table 2.

2.2. Data reduction

The data reduction was executed using the IRAF (Image Reduction and Analysis Facility) software package of NOAO. Following standard procedures, all the images were bias-subtracted and divided by a flat field. All the frames were carefully examined for cosmic rays or faint background sources at the vicinity of the target. If contaminated, the corresponding images were discarded.

For object photometry, we applied the aperture correction method (Howell, 1989) because the magnitude of the different targets was fainter than 20. In order to compute the PSF (Point Spread Function), we selected all the non-saturated and stellar shaped objects in the field. The PSF was deduced from an iterative procedure, which consisted in rejecting the PSF of objects obviously deviating from the mean PSF. This scheme allowed us to obtain a PSF representative of stellar objects. Since the TNO moves across the field of view, it is a little smeared and therefore does not have the same PSF as the star. To take into account this effect, we adjust the minimum size to use for the aperture correction method in function of the seeing and the object's trailing in order to have a deviation from stellar PSF less than 1% (McBride et al., 1999). As an example, with a seeing of $1''$ the minimum size of the photometric aperture (radius) to use on an object trailed by $0.5''$ is $1''$, and for a trailing of $1''$ the aperture size

Table 1
Observational circumstances

Object	Date	Δ (AU)	r (AU)	α (°)
1999 OX_3	2002 Jun 5	25.845	26.407	1.9
	2002 Jun 6	25.829	26.405	1.8
	2002 Jun 7	25.814	26.403	1.8
2000 OU_{69}	2002 Jun 6	40.496	41.087	1.0
2000 YW_{134}	2002 Oct 31	42.858	42.980	1.3
2001 FP_{185}	2002 Jun 6	33.994	34.276	1.6
2001 KA_{77}	2002 Jun 7	47.847	48.854	0.1
2001 KP_{77}	2002 Jun 5	35.024	36.011	0.4
2001 KY_{76}	2002 Jun 6	37.766	38.779	0.1
2001 QD_{298}	2002 Jun 7	40.659	41.079	1.3
2001 QF_{298}	2002 Oct 31	41.995	42.640	1.0
2001 QY_{297}	2002 Jun 5	42.002	42.577	1.1
2001 UO_{18}	2002 Oct 31	31.241	32.191	0.5
2001 UQ_{18}	2002 Oct 31	44.194	45.142	0.4
2001 UR_{163}	2002 Oct 31	48.054	49.009	0.3
2002 GF_{32}	2002 Jun 7	40.602	41.435	0.8
2002 GH_{32}	2002 Jun 6	41.558	42.330	0.9
	2002 Jun 7	41.569	42.330	0.9
2002 GJ_{32}	2002 Jun 5	41.852	42.661	0.8
2002 GP_{32}	2002 Jun 6	31.277	32.149	0.9
	2002 Jun 7	31.285	32.149	1.0
2002 GV_{32}	2002 Jun 7	31.543	32.422	0.9
2002 GZ_{32}	2002 Jun 5	20.832	21.117	2.7
2002 TX_{300}	2002 Oct 31	39.910	40.741	0.8

Notes: Coordinates are for the date of observations at 00 UT. r, Δ, α are, respectively, the heliocentric distance, the topocentric distance and the phase angle of the object (Minor Planet Ephemeris Service http://cfa-www.harvard.edu/iau/MPEph/MPEph.html).

should be 1.4″ wide. In our observations trailing was limited (long exposures were split), and we typically used an aperture of the size of the seeing disk for the objects and 5 times the FWHM for the aperture correction. The sky background was measured at a 5 pixel wide annulus centered on the object, at ∼ 6 FWHM from its center.

The stars from Landolt (1992) fields were observed and tracked during the night at different airmasses for absolute calibration. The photometric calibration parameters (zero point, extinction coefficients and color terms) were computed using the IRAF PHOTCAL package.

See Doressoundiram et al. (2002) for further details on the observational strategy and reduction techniques applied to the CFHT12K data.

3. Results

3.1. Colors, absolute magnitudes, and sizes

Table 3 presents the results obtained for the 20 recently observed objects. V magnitude and individual color measurements are given together with the corresponding UT date and time of observation. Photometric errors are based on photon noise, uncertainty of the aperture correction resulting from the dispersion among measurements of the different field stars, and calibration error. V, $B-V$, $V-R$, and $V-I$ (and associated errors) were derived simultaneously by solving equations relating instrumental and calibrated magnitudes. Finally, for each object, the shaded line indicates the weighted mean of the individual measurements. Hence, the computed final error could be less than individual error.

Table 2
Telescope/instrument characteristics

Telescope	Instruments		Filters		
	Detector	Pixel scale	Type	λ_c (nm)	FWHM (nm)
CFHT 3.6 m	CFH12K 12 MIT/LL 2KX4K	0.20″	Mould B	431.2	99.0
			Mould V	537.4	97.4
			Mould R	658.1	125.1
			Mould I	822.3	216.4

Table 4 gives a summary of the obtained averaged colors for the 71 objects in the 2MS dataset as well as other useful physical parameters derived from the observations: the absolute magnitude in the V band, H_V and the size.

Observations of TNOs are made at small phase angles where the opposition-brightening effect is likely to occur. Recent studies (Sheppard and Jewitt, 2002; Belskaya et al., 2003) have shown that this effect could be significant for TNOs and Centaurs. Absolute magnitudes (H_V) are computed using the linear phase function $\phi(\alpha) = 10^{-\alpha\beta}$:

$$H_V = V(1,1,0) = V - 5\log(r\Delta) - \alpha\beta.$$

Where V is the V-band magnitude, r is the object's heliocentric distance (AU), Δ is the object's geocentric distance (AU), α is the phase angle (deg) and β is the phase curve slope (mag/deg).

For TNOs we took the modal value of the measurements published by Sheppard and Jewitt (2002): $\beta = 0.14 \pm 0.03$. For Centaurs, we used a value of $\beta = 0.11 \pm 0.01$ obtained from a least-squares fit of the linear approximation $\phi(\alpha)$ to the published data by Bauer et al. (2002). These rather steep slopes show that the phase correction is important when calculating the absolute magnitude of TNOs. However, these numbers have to be considered as rough estimates due to low statistics. Sizes (in kilometer) have been estimated using an albedo of $p_R = 0.09$, considered as a better estimate by Brown and Trujillo (2004) instead of the usual 0.04 value. We should note that previously published absolute magnitude and size have been recomputed according to the new estimates on β and albedo adopted in this paper (see Table 4).

In Table 4 we report the name, classification and colors of each of the 2MS dataset. We have verified that our measurements agree quite well with the ones found in the literature, except for 2001 KA_{77} (4σ difference with the $V-I$ measurement of Peixinho et al., 2004) and 2000 YW_{134} (3σ difference with the $V-R$ measurement of Tegler et al., 2003; Peixinho et al., 2004).

3.2. TNO classifications

Apart from resonant objects there are no strict dynamical definitions for each family. We identify our resonant

Table 3
Individual color measurements

Object	V	Date (UT)	UT (B) (hr)[a]	$B-V$	UT (R) (hr)[a]	$V-R$	UT (I) (hr)[a]	$V-I$	Var[b]
1999 OX_3	22.05 ± 0.08	2002 Jun 5	12.317	0.99 ± 0.08	12.167	0.86 ± 0.04	12.467	1.33 ± 0.05	
	22.15 ± 0.06	2002 Jun 6	12.417	1.20 ± 0.08	12.271	0.73 ± 0.05	12.576	1.40 ± 0.05	YES[c]
	21.86 ± 0.06	2002 Jun 7	13.209	1.12 ± 0.06	13.062	0.70 ± 0.04	13.366	1.41 ± 0.04	
				1.11 ± 0.05		**0.76 ± 0.08**		**1.38 ± 0.02**	
2000 OU_{69}	23.42 ± 0.20	2002 Jun 6	–	–	12.800	0.70 ± 0.11	12.488	1.62 ± 0.16	
2000 YW_{134}	21.20 ± 0.05	2002 Oct 31	14.233	0.87 ± 0.04	14.086	0.37 ± 0.05	14.389	1.04 ± 0.03	
			14.720	0.87 ± 0.04	14.570	0.40 ± 0.03	14.875	1.10 ± 0.03	
				0.87 ± 0.03		*0.39 ± 0.03*		*1.07 ± 0.03*	
2001 FP_{185}	21.96 ± 0.08	2002 Jun 6	7.058	0.81 ± 0.06	6.912	0.64 ± 0.04	7.214	0.97 ± 0.04	
			7.541	0.89 ± 0.06	7.393	0.58 ± 0.04	7.696	1.12 ± 0.05	YES
				0.85 ± 0.04		*0.61 ± 0.03*		*1.05 ± 0.06*	
2001 KA_{77}	22.49 ± 0.08	2002 Jun 7	11.809	1.25 ± 0.10	11.629	0.72 ± 0.06	12.031	1.52 ± 0.06	
2001 KP_{77}	23.21 ± 0.24	2002 Jun 5	9.733	0.89 ± 0.16	9.550	0.61 ± 0.11	9.950	0.97 ± 0.09	
			10.383	0.95 ± 0.25	–	–	–	–	
				0.91 ± 0.13		*0.61 ± 0.11*		*0.97 ± 0.09*	
2001 KY_{76}	22.93 ± 0.25	2002 Jun 6	10.273	1.39 ± 0.16	–	–	10.95	1.12 ± 0.12	
			10.922	1.55 ± 0.26	10.741	0.41 ± 0.13	11.144	0.95 ± 0.12	
				1.43 ± 0.14		*0.41 ± 0.13*		*1.03 ± 0.08*	
2001 QD_{298}	22.97 ± 0.08	2002 Jun 7	14.153	0.97 ± 0.13	13.973	0.67 ± 0.09	–	–	
2001 QF_{298}	21.75 ± 0.10	2002 Oct 31	7.558	0.67 ± 0.06	7.443	0.33 ± 0.06	7.665	0.68 ± 0.06	
			7.909	0.59 ± 0.05	7.793	0.42 ± 0.05	8.016	0.75 ± 0.08	
				0.63 ± 0.04		*0.38 ± 0.04*		*0.71 ± 0.05*	
2001 QY_{297}	21.82 ± 0.23	2002 Jun 5	12.850	0.65 ± 0.18	12.667	0.44 ± 0.14	13.067	0.88 ± 0.10	
			13.500	0.74 ± 0.16	13.317	0.43 ± 0.11	13.717	1.32 ± 0.16	YES
				0.70 ± 0.12		*0.43 ± 0.09*		*1.10 ± 0.19*	
2001 UO_{18}	23.62 ± 0.31	2002 Oct 31	10.558	1.30 ± 0.30	10.409	0.91 ± 0.19	10.716		
			11.048	1.25 ± 0.30	10.899	0.70 ± 0.18	11.205		
				1.27 ± 0.21		*0.79 ± 0.13*			
2001 UQ_{18}	23.12 ± 0.21	2002 Oct 31	11.569	0.91 ± 0.13	11.421	0.73 ± 0.11	11.726	1.38 ± 0.17	
			12.062		11.913	0.74 ± 0.11	12.219	1.10 ± 0.10	
				0.91 ± 0.13		*0.74 ± 0.08*		*1.17 ± 0.09*	
2001 UR_{163}	21.55 ± 0.07	2002 Oct 31	9.517	1.43 ± 0.06	9.402	0.79 ± 0.04	9.623	1.64 ± 0.04	
			9.851	1.45 ± 0.06	10.084	0.89 ± 0.04	9.956	1.58 ± 0.04	
				1.44 ± 0.04		*0.84 ± 0.03*		*1.61 ± 0.03*	
2002 GF_{32}	22.97 ± 0.13	2002 Jun 7	7.449	0.95 ± 0.11	7.268	0.83 ± 0.08	7.671	1.33 ± 0.07	
			8.097	1.01 ± 0.11	7.917	0.74 ± 0.07	8.320	1.26 ± 0.07	
				0.98 ± 0.08		*0.78 ± 0.05*		*1.29 ± 0.05*	
2002 GH_{32}	23.22 ± 0.24	2002 Jun 6	8.113	0.68 ± 0.08	7.965	0.74 ± 0.15	8.268	1.13 ± 0.12	
			8.594	0.60 ± 0.18	8.447	0.91 ± 0.13	8.750	1.23 ± 0.12	
				0.64 ± 0.13		*0.84 ± 0.10*		*1.18 ± 0.08*	
2002 GJ_{32}	22.53 ± 0.13	2002 Jun 5	8.083	0.82 ± 0.11	8.967	0.68 ± 0.08	9.200	1.65 ± 0.10	
2002 GP_{32}	22.06 ± 0.10	2002 Jun 6	9.130	1.14 ± 0.07	8.983	0.49 ± 0.06	9.285	0.98 ± 0.06	
			9.613	1.13 ± 0.07	9.465	0.44 ± 0.06	9.768	0.93 ± 0.06	
				1.14 ± 0.05		*0.47 ± 0.04*		*0.94 ± 0.04*	
	22.01 ± 0.05	2002 Jun 7	9.929	0.73 ± 0.05	9.083	0.20 ± 0.04	9.385	0.88 ± 0.05	YES
2002 GV_{32}	22.68 ± 0.12	2002 Jun 7	–	–	9.580	0.82 ± 0.05	9.981	1.48 ± 0.06	
			10.410	1.21 ± 0.10	10.228	0.65 ± 0.07	10.632	1.49 ± 0.07	
				1.21 ± 0.10		*0.75 ± 0.04*		*1.48 ± 0.05*	
2002 GZ_{32}	20.96 ± 0.06	2002 Jun 5	7.483	0.71 ± 0.03	7.300	0.58 ± 0.02	7.400	0.98 ± 0.02	
			7.717	0.67 ± 0.04	7.617	0.45 ± 0.10	7.667	0.85 ± 0.02	YES
			8.050	0.80 ± 0.04	7.883	0.51 ± 0.03	7.983	0.92 ± 0.03	
				0.73 ± 0.06		*0.51 ± 0.04*		*0.92 ± 0.05*	
2002 TX_{300}	19.76 ± 0.02	2002 Oct 31	8.901	0.62 ± 0.02	8.807	0.37 ± 0.02	8.977	0.70 ± 0.02	
			9.173	0.65 ± 0.02	9.081	0.35 ± 0.02	9.251	0.67 ± 0.03	
				0.63 ± 0.02		*0.36 ± 0.02*		*0.69 ± 0.02*	

Notes: Individual $B-V$, $V-R$, $V-I$ color index are indicated as well as their 1σ error. For each object, the line in bold indicates the weighted mean of the individual measurements. In the case where significant color variation is detected (flagged as "yes" in last column) a simple mean is adopted and the uncertainty is the quadratic of the errors.

[a] UT start time in hour of the corresponding B, R, or I exposure.

[b] This column indicates whether a true (no rotation effect) color variation is detected.

[c] Color different from previous measurement (Doressoundiram et al., 2001).

Table 4
Mean colors and estimated size of Centaurs and TNOs

Object	Group[a]	V	$B-V$	$V-R$	$V-I$	H_V[b]	Size[c]	Ref.
Solar colors			0.67	0.36	0.69			
10370 Hylonome	Centaur	22.59 ± 0.08	0.77 ± 0.08	0.38 ± 0.06	0.91 ± 0.09	9.48 ± 0.10	57	g
1993 FW	Clas I/Clas II	23.47 ± 0.02	1.01 ± 0.09	0.66 ± 0.04	1.05 ± 0.09	7.14 ± 0.03	192	e
1994 JR_1	Plutino	23.30 ± 0.30	1.01 ± 0.18	0.60 ± 0.12	1.72 ± 0.12	7.66 ± 0.30	147	d
1994 TB	Plutino	22.00 ± 0.30	1.10 ± 0.18	0.74 ± 0.11	1.46 ± 0.08	7.12 ± 0.30	201	d
1995 HM_5	Plutino	23.40 ± 0.02	0.67 ± 0.06	0.55 ± 0.04	0.92 ± 0.11	8.20 ± 0.03	112	e
1995 QY_9	Plutino	22.20 ± 0.30	0.74 ± 0.20	0.47 ± 0.12		7.49 ± 0.30	149	d
1995 SM_{55}	Clas I/SDO II	20.61 ± 0.02	0.66 ± 0.03	0.40 ± 0.03	0.78 ± 0.03	4.50 ± 0.03	574	g
1995 TL_8	SDO I/SDO II	21.71 ± 0.05	0.68 ± 0.05	0.40 ± 0.05	0.67 ± 0.05	5.29 ± 0.06	399	g
1996 TK_{66}	Clas I/Clas II	22.95 ± 0.05	0.95 ± 0.08	0.81 ± 0.05	1.42 ± 0.06	6.52 ± 0.05	274	g
1996 TL_{66}	SDO I/SDO II	21.00 ± 0.30	0.74 ± 0.08	0.44 ± 0.05	0.70 ± 0.07	5.36 ± 0.30	394	d
1996 TO_{66}	Clas I/SDO II	21.20 ± 0.30	0.72 ± 0.07	0.40 ± 0.04	0.78 ± 0.04	4.56 ± 0.30	560	d
1996 TP_{66}	Plutino	21.20 ± 0.30	1.14 ± 0.14	0.65 ± 0.13	1.08 ± 0.14	6.79 ± 0.30	224	d
1997 CQ_{29}	Clas I/Clas II	23.53 ± 0.02	0.99 ± 0.12	0.68 ± 0.06	1.30 ± 0.09	7.38 ± 0.02	173	e
1997 CR_{29}	Clas I/SDO II	23.71 ± 0.08	0.79 ± 0.10	0.47 ± 0.08	1.15 ± 0.12	7.42 ± 0.08	155	f
1997 CS_{29}	Clas I/Clas II	21.97 ± 0.03	1.05 ± 0.06	0.66 ± 0.02	1.19 ± 0.04	5.53 ± 0.03	402	e
1997 CU_{29}	Clas I/Clas II	23.25 ± 0.06	1.05 ± 0.10	0.66 ± 0.06	1.22 ± 0.06	6.78 ± 0.06	227	f
1998 BU_{48}	Centaur	21.53 ± 0.03	1.01 ± 0.04	0.64 ± 0.03	1.17 ± 0.04	7.01 ± 0.03	202	g
1998 FS_{144}	Clas I/Clas II	23.39 ± 0.03	0.91 ± 0.08	0.56 ± 0.07		7.14 ± 0.03	184	e
1998 HK_{151}	Plutino	22.24 ± 0.03	0.72 ± 0.05	0.52 ± 0.04	0.88 ± 0.05	7.30 ± 0.03	167	g
1998 KG_{62}	Clas I/Clas II	23.55 ± 0.05	1.00 ± 0.06	0.53 ± 0.05	1.17 ± 0.04	6.88 ± 0.05	204	f
1998 QM_{107}	Centaur	23.22 ± 0.06		0.68 ± 0.06		10.76 ± 0.06	37	g
1998 SG_{35}	Centaur	21.43 ± 0.06	0.89 ± 0.11	0.43 ± 0.08	1.02 ± 0.08	11.04 ± 0.06	29	f
1998 SN_{165}	Clas I/SDO II	21.55 ± 0.06	0.82 ± 0.08	0.33 ± 0.08	0.84 ± 0.08	5.65 ± 0.06	327	f
1998 TF_{35}	Centaur	22.11 ± 0.04	1.17 ± 0.05	0.71 ± 0.04	1.41 ± 0.04	9.18 ± 0.04	77	g
1998 VG_{44}	Plutino	21.56 ± 0.04	0.89 ± 0.05	0.58 ± 0.04	1.08 ± 0.05	6.67 ± 0.04	230	g
1998 WH_{24}	Clas I/Clas II	21.31 ± 0.05	0.95 ± 0.03	0.63 ± 0.03	1.25 ± 0.04	4.99 ± 0.05	509	g
1998 WW_{24}	Plutino	23.43 ± 0.05	0.69 ± 0.08	0.42 ± 0.06	1.15 ± 0.07	8.33 ± 0.05	99	g
1999 CC_{158}	SDO I/SDO II	22.16 ± 0.03	1.01 ± 0.04	0.63 ± 0.03	1.28 ± 0.04	5.79 ± 0.04	352	g
1999 CD_{158}	Clas I/SDO II	22.09 ± 0.03	0.86 ± 0.04	0.54 ± 0.03	1.13 ± 0.04	5.20 ± 0.03	443	g
1999 CL_{158}	SDO I/SDO II	22.32 ± 0.05	0.80 ± 0.06	0.39 ± 0.04	0.86 ± 0.06	6.90 ± 0.05	189	g
1999 DE_9	5:2	20.67 ± 0.03	0.94 ± 0.03	0.59 ± 0.03	1.17 ± 0.03	5.18 ± 0.03	458	g
1999 DF_9	Clas I/Clas II	22.48 ± 0.06	0.92 ± 0.06	0.71 ± 0.05	1.36 ± 0.06	6.33 ± 0.06	286	g
1999 HB_{12}	5:2	22.67 ± 0.04	0.87 ± 0.06	0.50 ± 0.05	0.82 ± 0.08	7.07 ± 0.05	184	f
1999 HR_{11}	Clas I/Clas II	23.94 ± 0.05	0.92 ± 0.12	0.53 ± 0.10	1.33 ± 0.07	7.52 ± 0.05	152	f
1999 HS_{11}	Clas I/Clas II	23.41 ± 0.05	1.01 ± 0.16	0.68 ± 0.10	1.28 ± 0.09	6.93 ± 0.05	213	f
1999 OX_3	Centaur	22.02 ± 0.10	1.11 ± 0.05	0.76 ± 0.08	1.38 ± 0.02	7.60 ± 0.10	162	h
1999 OX_3		22.15 ± 0.05	1.21 ± 0.07	0.62 ± 0.05	1.43 ± 0.05	7.77 ± 0.05	141	g
1999 OY_3	Clas I/SDO II	22.47 ± 0.03	0.75 ± 0.03	0.26 ± 0.03	0.57 ± 0.04	6.54 ± 0.03	210	g
1999 RY_{215}	SDO I/SDO II	22.99 ± 0.06	0.80 ± 0.10	0.48 ± 0.05	1.26 ± 0.08	7.21 ± 0.06	171	f
1999 TC_{36}	Plutino	20.49 ± 0.05	0.99 ± 0.09	0.65 ± 0.06	1.37 ± 0.07	5.37 ± 0.05	432	f
1999 TD_{10}	SDO I/SDO II	20.09 ± 0.02	0.72 ± 0.02	0.51 ± 0.02	1.06 ± 0.03	8.53 ± 0.02	94	g
1999 UG_5	Centaur	19.73 ± 0.01	1.05 ± 0.02	0.64 ± 0.02	1.29 ± 0.03	10.44 ± 0.01	42	g
1999 XX_{143}	Centaur	23.00 ± 0.05	1.02 ± 0.06	0.59 ± 0.04	1.01 ± 0.04	9.03 ± 0.05	78	g
2000 EB_{173}	Plutino	20.00 ± 0.01	0.96 ± 0.02	0.53 ± 0.01	1.19 ± 0.01	5.05 ± 0.03	474	f
2000 FE_8	5:2	22.59 ± 0.05	0.75 ± 0.06	0.48 ± 0.04	0.98 ± 0.05	6.86 ± 0.05	201	g
2000 GP_{183}	Plutino	21.96 ± 0.05	0.77 ± 0.04	0.39 ± 0.04	0.82 ± 0.04	6.06 ± 0.05	279	g
2000 OJ_{67}	Clas I/Clas II	22.93 ± 0.07	1.05 ± 0.06	0.67 ± 0.05	1.27 ± 0.07	6.54 ± 0.07	255	g
2000 OK_{67}	Clas I/Clas II	22.81 ± 0.07	0.89 ± 0.08	0.65 ± 0.05	1.22 ± 0.08	6.57 ± 0.07	249	g
2000 OU_{69}	Clas I/Clas II	23.42 ± 0.20	–	0.70 ± 0.11	1.62 ± 0.16	7.18 ± 0.20	192	h
2000 PE_{30}	SDO I/SDO II	22.04 ± 0.04	0.71 ± 0.05	0.38 ± 0.04	0.83 ± 0.04	6.13 ± 0.04	269	f
2000 QC_{243}	Centaur	20.31 ± 0.03	0.67 ± 0.03	0.44 ± 0.03	0.91 ± 0.03	7.47 ± 0.03	149	g
2000 WR_{106} (Varuna)	Clas I/Clas II	20.34 ± 0.02	0.92 ± 0.03	0.61 ± 0.02	1.22 ± 0.02	4.02 ± 0.02	788	g
2000 YW_{134}	SDO I / SDO II	21.20 ± 0.05	0.87 ± 0.03	0.39 ± 0.03	1.07 ± 0.03	4.69 ± 0.05	524	h
2001 FP_{185}	SDO I/SDO II	21.96 ± 0.08	0.85 ± 0.04	0.61 ± 0.03	1.05 ± 0.06	6.41 ± 0.08	262	h
2001 KA_{77}	Clas I/Clas II	22.49 ± 0.08	1.25 ± 0.10	0.72 ± 0.06	1.52 ± 0.06	5.64 ± 0.08	394	h
2001 KA_{77}		22.66 ± 0.05	1.05 ± 0.05	0.67 ± 0.04	1.48 ± 0.04	5.64 ± 0.05	394	g
2001 KD_{77}	Plutino	21.97 ± 0.02	1.12 ± 0.03	0.65 ± 0.04	1.22 ± 0.05	6.31 ± 0.02	280	g
2001 KP_{77}	7:4	23.21 ± 0.24	0.91 ± 0.13	0.61 ± 0.11	0.97 ± 0.09	7.65 ± 0.23	146	h
2001 KX_{76}	Plutino	20.39 ± 0.02	1.03 ± 0.03	0.61 ± 0.03	1.19 ± 0.04	3.86 ± 0.02	849	g

(*continued on next page*)

Table 4 (*continued*)

Object	Group[a]	V	$B-V$	$V-R$	$V-I$	H_V[b]	Size[c]	Ref.
2001 KY_{76}	Plutino	22.93 ± 0.25	1.43 ± 0.14	0.41 ± 0.13	1.03 ± 0.08	7.09 ± 0.25	175	h
2001 QD_{298}	Clas I/Clas II	22.97 ± 0.08	0.97 ± 0.13	0.67 ± 0.09	–	6.67 ± 0.08	239	h
2001 QF_{298}	Plutino	21.75 ± 0.10	0.63 ± 0.04	0.38 ± 0.04	0.71 ± 0.04	5.34 ± 0.10	386	h
2001 QY_{297}	Clas I/Clas II	21.82 ± 0.23	0.70 ± 0.12	0.43 ± 0.09	1.10 ± 0.19	5.40 ± 0.23	384	h
2001 UO_{18}	Plutino	23.62 ± 0.31	1.27 ± 0.21	0.79 ± 0.13	–	8.54 ± 0.31	107	h
2001 UQ_{18}	Clas I/Clas II	23.12 ± 0.21	0.91 ± 0.13	0.74 ± 0.08	1.17 ± 0.09	6.56 ± 0.21	260	h
2001 UR_{163}	SDO I/SDO II	21.55 ± 0.07	1.44 ± 0.04	0.84 ± 0.03	1.61 ± 0.03	4.65 ± 0.07	656	h
2002 GF_{32}	Clas I/Clas II	22.97 ± 0.13	0.98 ± 0.08	0.78 ± 0.05	1.29 ± 0.05	6.73 ± 0.13	245	h
2002 GH_{32}	Clas I/Clas II	23.17 ± 0.28	0.64 ± 0.13	0.84 ± 0.10	1.18 ± 0.08	6.81 ± 0.28	243	h
2002 GJ_{32}	Clas I/Clas II	22.53 ± 0.13	0.82 ± 0.11	0.68 ± 0.08	1.65 ± 0.10	6.16 ± 0.13	305	h
2002 GP_{32}	5:2	22.04 ± 0.11	0.94 ± 0.07	0.34 ± 0.06	0.91 ± 0.06	6.90 ± 0.11	185	h
2002 GV_{32}	Plutino	22.68 ± 0.12	1.21 ± 0.10	0.75 ± 0.04	1.48 ± 0.05	7.50 ± 0.12	169	h
2002 GZ_{32}	Centaur	20.96 ± 0.06	0.73 ± 0.06	0.51 ± 0.04	0.92 ± 0.05	7.48 ± 0.05	153	h
2002 TX_{300}	Clas I/SDO II	19.76 ± 0.02	0.63 ± 0.02	0.36 ± 0.02	0.69 ± 0.02	3.59 ± 0.02	857	h

[a] Groups are indicated following the two classification schemes described in Section 3.
[b] H_V = revised absolute V magnitude (corrected from phase angle).
[c] The equivalent diameter has been derived from the absolute magnitude and assuming an albedo of $p_R = 0.09$.
[d] Barucci et al. (1999).
[e] Barucci et al. (2000).
[f] Doressoundiram et al. (2001).
[g] Doressoundiram et al. (2002).
[h] This work.

objects according to Chiang et al. (2003a, 2003b). Centaurs and scattered disk objects (SDOs) are grouped together on the Minor Planet Center (http://cfa-www.harvard.edu/iau/Ephemerides/Distant/index.html) with no distinction. From this list we consider Centaurs as those with perihelia (q) below 30 AU (Neptune's semi-major axis) and aphelia (Q) below 48 AU (2:1 resonance), the others we classify as SDOs.

The distinction between Classical objects and SDOs is even more delicate, since it influences critically the correlations found among each family. From the Minor Planet Center list of TNOs all non-resonant objects will be considered as either Classicals or SDOs (to be added to the previous ones) according to two different classification schemes:

Classif. I. Since objects with $q < 35$ AU enter Neptune's Hill sphere, and therefore may be unstable (Torbett and Smoluchowski, 1990), we consider as Classical objects all non-resonant objects with semi-major axis between the 3:2 and 2:1 resonances (39.5 AU $< a <$ 48 AU) and perihelion $q > 35$ AU. From Duncan et al. (1995) objects with low inclined orbits, $q > 36$ AU and 36 AU $< a <$ 40 AU are also stable and included in the Classicals. The remaining objects are defined as SDOs.

Classif. II. Kuchner et al. (2002) extended the Duncan et al. (1995) classification in order to include higher orbital inclinations. They found that there are inclination dependent instabilities under which objects with $q < 39$ AU may still be largely perturbed. Therefore, as a second approach, all Classicals from Classif. I with $q < 39$ AU are classified as SDOs.

In the 20 objects of our sample, we have 2 Centaurs, 4 Plutinos, 8 or 9 Classical TNOs (depending on classification scheme), 3 or 4 Scattered TNOs (idem) and 2 TNOs located in the 5:2 and 7:4 mean motion resonances with Neptune (see column 2 of Table 4).

In this study, we have merged our most recent sample of 20 objects with data collected by our group since 1999 (Barucci et al., 1999, 2000; Doressoundiram et al. 2001, 2002), the so-called Meudon Multicolor Survey (2MS). The 2MS sample has colors for 71[1] Centaurs and TNOs, thus constituting one of the largest *homogeneous* (same observational strategy and data reduction procedure) datasets collected so far for the Edgeworth–Kuiper belt (EKB). In Table 4 we report the name, classification and colors of each object in the 2MS dataset.

3.3. Color variation

Surface homogeneity or heterogeneity is an important issue as it is a prediction of the proposed collision resurfacing scenario (Luu and Jewitt, 1996; Jewitt and Luu, 2001). According to this model, object surfaces should display large color variation as the result of two competing resurfacing mechanisms: reddening by cosmic irradiation and bluing by cratering collisions. Thus, on a single object, large variations in color could potentially exist if the surface contains some regions that are dominated by more neutral, freshly exca-

[1] Currently, the 2MS dataset comprises measurements of 71 objects (at least the $V-R$ color), and 65 of them have the complete set of *BVRI* colors, and 69 have the *BVR* colors. Moreover, on these 71 individual objects, some have been observed several times on different runs (1999 OX_3 and 2001 KA_{77}).

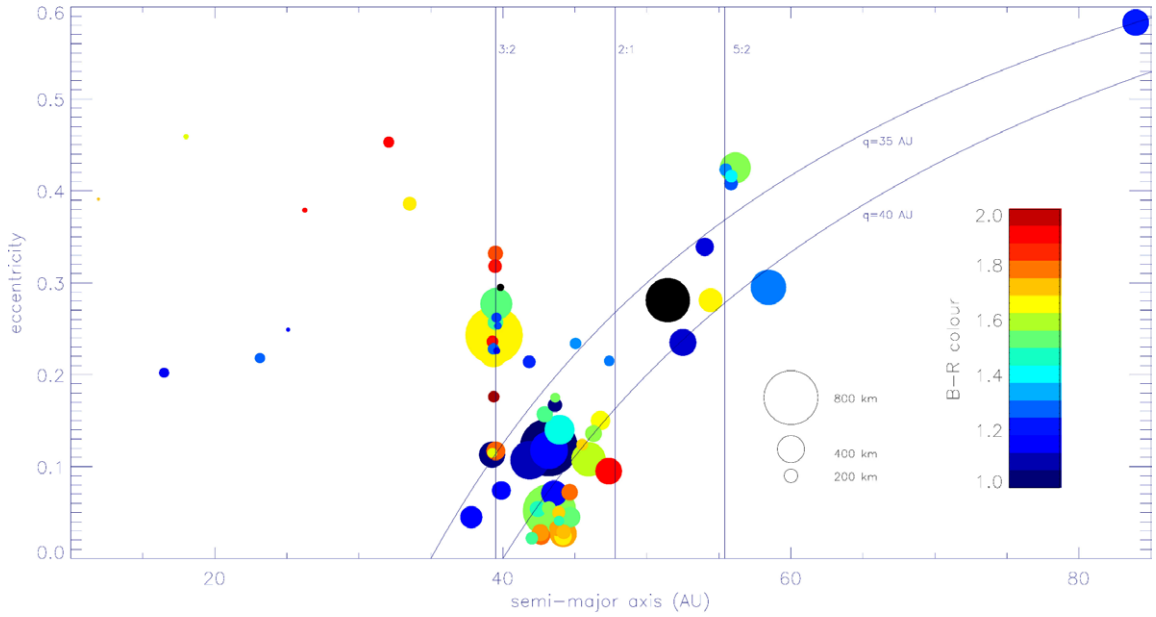

Fig. 1. Colors of TNOs and Centaurs (69 objects) in the orbital eccentricity versus semi-major axis plane. The advantage of this representation is that it offers to the eye the global color distribution of the TNOs. The sizes of the symbols are proportional to the corresponding object's diameter. A color palette has been adopted to scale the color spread from $B-R=1.0$ (coded as dark blue) to $B-R=2.0$ (coded as red). In comparison, $B-R=1.03$ for the Sun and about 2 for the Centaur 5145 Pholus (one of the reddest known object in the Solar System). 3:2 ($a\sim 39.5$ AU), 2:1 ($a\sim 48$ AU), and 5:2 ($a\sim 55.4$ AU) resonances with Neptune are marked, as well as the $q=40$ AU perihelion curve. The very red objects (see text) 2001 UO_{18} ($B-R=2.06$) and 2001 UR_{163} ($B-R=2.28$) have been coded in black in order to keep a readable color range.

vated material while other regions are dominated by redder long-term irradiated material.

By performing two (in most of our observations) photometric sequences over a significant time span to obtain color indices corresponding to different parts of the surface of the rotating object, we could monitor for possible color variation. This occurred a few times, where the differences between the measurements were significant in comparison with the uncertainties. These objects are flagged as "yes" in the last column of Table 3. We checked that these differences were not due to reduction or observational (contamination) problems. The objects that show color variations are: 1999 OX_3 (color different from previous measurement from Doressoundiram et al., 2002, hereafter DOR02), 2001 FP_{185}, 2001 QY_{297}, 2002 GP_{32}, 2002 GZ_{32}. However, most of these color variations are below the 2σ level.

To date, no such large color variation has been identified (see also objects with color variation highlighted in DOR02, and also in Tegler et al., 2003). Recent work by Delsanti et al. (2004) involving collisions plus resurfacing by ice-recondensation produced by outgassing activity, predicted that such color variation should occur on small objects. The objects highlighted in this work should be prime targets for further observations in order to study and confirm the color variation with the rotation.

3.4. Color distribution

The $B-R$ color versus orbital parameters is shown in Figs. 1 and 2 similar to the plots of Doressoundiram et al. (2001) and DOR02 that have become our norm for identifying structures and trends in the color distribution. Objects are plotted as a function of their orbital parameters, with circles proportional to their estimated size. The color of circles is scaled from blue to red according to their $B-R$ color index. The very red objects (see below) 2001 UO_{18} ($B-R=2.06$) and 2001 UR_{163} ($B-R=2.28$) have been coded in black in order to keep a readable color range.

Looking at Fig. 1 it is visually clear that, apart from 3:2 resonants (Plutinos) and Centaurs, objects with smaller perihelia (i.e., objects above the $q=40$ AU line) tend to be bluer and all objects with perihelia above 40 AU (i.e., objects below the $q=40$ AU line) are redder. In Fig. 2, it is visually clear that high inclination objects tend to be bluer than low inclination ones. However, as we will see below, this result may be connected with perihelion. We also see that larger objects possess higher inclination values, but statistically we cannot detect a correlation.

3.5. The reddest objects

In our sample, two objects are very red objects: 2001 UO_{18} ($B-R=2.06$) and 2001 UR_{163} ($B-R=2.28$). 2001 UR_{163} is even redder than the two reddest known objects in the Solar System, the Centaur Pholus (averaged $B-R=2.09$ and $V-I=1.6$ from MBOSS data base http://www.sc.eso.org/~ohainaut/MBOSS/mbossColors.html) and the Comet C/2001 T4 ($V-I=1.7$, see Bauer et al., 2003a). However in the case of Comet C/2001 T4, its red color

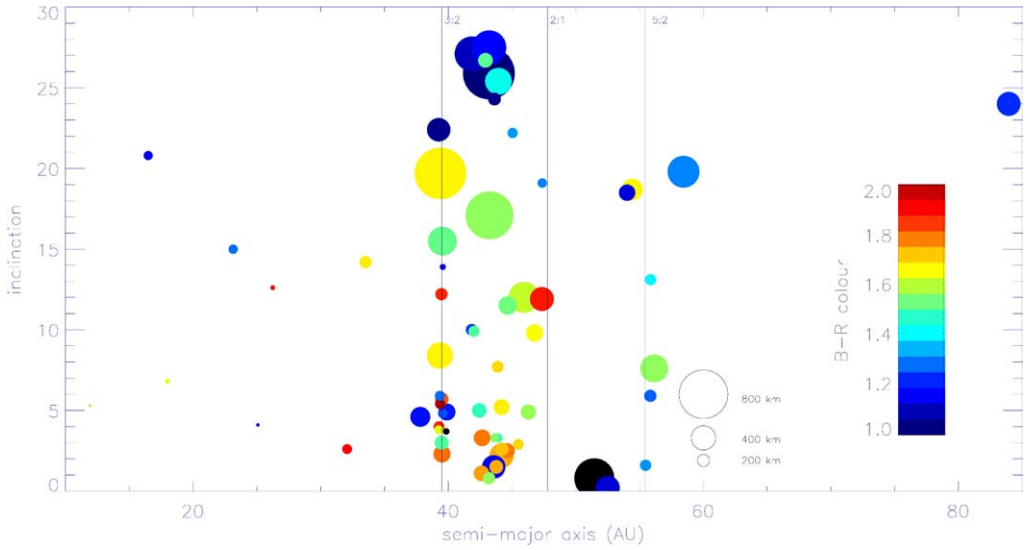

Fig. 2. Same as Fig. 1 in the orbital inclination versus semi-major axis plane.

does not reflect the color of the nucleus since measurements should have been contaminated by the active coma.

4. Correlations

As in our previous work based on a sample of 52 color data, we performed intensive statistical analysis on 69 objects in our extended dataset of 71 (2001 KA_{77} was discarded from the analysis due to excessive variation from previous observations, and also 1998 QM_{107} since it was only observed in $V - R$). We investigated the correlations between color and orbital and physical characteristics within each of the EKB dynamical families. In general, we confirmed almost all the correlations and trends found in the DOR02 paper. The obtained results of this analysis are listed on Tables 5 and 6.

We looked for evidence of correlations, and their significance levels (SL) using only Spearman-rank correlation (Spearman, 1904) and consider those correlations with r greater than 0.6 to be strong, values of r between 0.3 and 0.6 indicate a possible weak correlation, and values less than 0.3 indicate no correlation.

Spearman correlation discards some information from the data, by ranking values instead of using their absolute value, making it less powerful than Pearson correlation. Nonetheless, it is distribution-free, making it more robust than Pearson correlation that looses its validity under non-Gaussian distributions. Present statistics show no evidence for Gaussian distributions of colors or orbital parameters; therefore we consider more adequate to use Spearman correlation. This method is also less sensitive to outliers. Another advantage is the capability to compute precisely the significance level (SL) of a measured correlation coefficient even for small samples. This SL may be interpreted as the probability P that the measured correlation value r could have been obtained from an uncorrelated set of data. We want a SL as high as possible (preferably above the "canonical" 3σ level, i.e., SL $> 3\sigma$, or equivalently $P < 0.003$). Nevertheless, rejecting categorically a correlation if SL does not reach 3σ will result in loosing all kind of possible insights to the understanding of what is really going on. Therefore, we discuss our 2σ results here but with the knowledge that these results are more likely to change significantly (either becoming stronger or weaker) in the future with more observations.

Another important issue, particularly when we are dealing with small samples, is the risk factor, β. That is, the probability of not seeing a correlation when actually it is present in the parent population. By setting the risk factor to the standard $\beta = 0.20$, we may compute the sample size needed to detect, at a certain SL, different correlation values. For example, with a 20% probability of failing to detect a correlation of $r = 0.6$, with $P = 0.05$ (i.e., SL $= 2\sigma$), a minimum of 20 objects are needed (to detect it at 3σ, we need 34). This does not mean that a strong correlation cannot be found with fewer objects, it means only that a risk of failing to detect such correlation is greater.

4.1. Centaur ($N = 9$)

Centaurs reveal evidence for correlations between colors and orbital eccentricity. There is strong evidence for a correlation for $B - V$ and e ($r = 0.78$, 2.5σ), but it does not reach our acceptance limits between $V - R$ and e ($r = 0.64$, 1.9σ), and appears non-existent for $R - I$ ($r = 0.33$, 0.9σ). However, with weaker significance, $B - R$ shows possible evidence of a correlation with e ($r = 0.72$, 2.2σ). These results are stronger than found by DOR02, but the significance level does not allow a clear confirmation. Peixinho et al. (2004), also found evidence for a strong $B - V$ versus e correlation, with a larger dataset ($N = 14$), but no

Table 5
Correlation's values for Centaurs, Plutinos, and SDOs

Quantity[a]	Quantity[a]	Group[b]	r_{corr}[c]	Prob[d]	SL[e]
$B-V$	$V-R$	Centaurs ($N=9$)	0.82	0.007	2.7
$B-V$	$R-I$	Centaurs ($N=9$)	0.75	0.02	2.3
$V-R$	$R-I$	Centaurs ($N=9$)	0.52	0.15	1.4
$B-R$	q	Centaurs ($N=9$)	−0.07	0.86	0.2
$B-V$	e	Centaurs ($N=9$)	0.78	0.01	2.5
$B-R$	e	Centaurs ($N=9$)	0.72	0.03	2.2
$B-I$	e	Centaurs ($N=9$)	0.73	0.02	2.2
$V-R$	e	Centaurs ($N=9$)	0.64	0.06	1.9
$V-I$	e	Centaurs ($N=9$)	0.62	0.08	1.8
$R-I$	e	Centaurs ($N=9$)	0.33	0.39	0.9
$B-R$	a	Centaurs ($N=9$)	0.40	0.29	1.1
$B-R$	i	Centaurs ($N=9$)	−0.48	0.19	1.3
$B-V$	$V-R$	Plutinos ($N=17$)	0.65	0.005	2.8
$B-V$	$R-I$	Plutinos ($N=15$)	0.44	0.10	1.7
$V-R$	$R-I$	Plutinos ($N=15$)	0.45	0.09	1.7
$B-R$	H	Plutinos ($N=17$)	−0.00	0.99	0.0
$B-R$	q	Plutinos ($N=17$)	−0.36	0.15	1.4
$B-R$	e	Plutinos ($N=17$)	0.37	0.14	1.5
$B-R$	a	Plutinos ($N=17$)	−0.15	0.57	0.6
$B-R$	i	Plutinos ($N=17$)	−0.31	0.23	1.2
$B-V$	$V-R$	Scattered I ($N=10$)	0.59	0.07	1.8
$B-V$	$R-I$	Scattered I ($N=10$)	0.69	0.03	2.2
$V-R$	$R-I$	Scattered I ($N=10$)	0.47	0.17	1.4
$B-R$	q	Scattered I ($N=10$)	0.01	0.99	0.0
$B-R$	e	Scattered I ($N=10$)	0.00	1.00	0.0
$B-R$	a	Scattered I ($N=10$)	0.05	0.88	0.1
$B-R$	i	Scattered I ($N=10$)	0.22	0.53	0.6
$B-V$	$V-R$	Scattered II ($N=17$)	0.49	0.04	2.0
$B-V$	$R-I$	Scattered II ($N=17$)	0.68	0.003	3.0
$V-R$	$R-I$	Scattered II ($N=17$)	0.50	0.04	2.0
$B-R$	q	Scattered II ($N=17$)	−0.13	0.63	0.5
$B-R$	e	Scattered II ($N=17$)	0.44	0.07	1.8
$B-R$	a	Scattered II ($N=17$)	0.46	0.06	1.8
$B-R$	i	Scattered II ($N=17$)	−0.15	0.56	0.6

[a] a = semi-major axis, e = eccentricity, i = inclination, q = perihelion, H absolute magnitude.

[b] Dynamical class, according to Section 3, and number of measurements in the sample.

[c] Spearman's rank correlation statistic.

[d] Probability of obtaining a higher or equal coefficient of correlation from an uncorrelated set of data. $P < 0.003$ indicates a correlation with $> 3\sigma$ significance level (SL).

[e] Significance level (SL) of the correlation, derived from the probability and assuming Gaussian statistics. $P = 0.01$ means a 2.6σ significance. $P = 0.001$ confidence means a 3.3σ significance.

$B-R$ versus e correlation. Bauer et al. (2003b) with a sample of 24 Centaurs in $V-R$ and $R-I$ colors, have not detected any correlation with eccentricity, nonetheless, they found very strong evidence for $V-R$ and $R-I$ correlation with a, while we do not detect it among our small sample.

We also find strong color correlations for $B-V$ versus $V-R$ and $B-V$ versus $R-I$, but see no evidence for a correlation between $V-R$ and $R-I$. We recall, however, that sampling is very small ($N \ll 20$) and the risk factor of not detecting a correlation of $r = 0.6$ is 60%. The risk factor is lower than 20% only for correlations stronger than $r = 0.87$.

Table 6
Correlation's values for Classical objects

Quantity[a]	Quantity[a]	Group[b]	r_{corr}[c]	Prob[d]	SL[e]
$B-V$	$V-R$	Classicals I ($N=27$)	0.47	0.01	2.5
$B-V$	$R-I$	Classicals I ($N=25$)	0.21	0.32	1.0
$V-R$	$R-I$	Classicals I ($N=25$)	0.20	0.32	1.0
$B-V$	q	Classicals I ($N=27$)	0.52	0.0052	2.8
$V-R$	q	Classicals I ($N=28$)	0.67	0.0001	3.9
$R-I$	q	Classicals I ($N=26$)	0.15	0.46	0.7
$V-I$	q	Classicals I ($N=26$)	0.55	0.0037	2.9
$B-R$	q	Classicals I ($N=27$)	0.65	0.0002	3.7
$B-I$	q	Classicals I ($N=25$)	0.61	0.0012	3.2
$B-V$	e	Classicals I ($N=27$)	−0.33	0.091	1.7
$V-R$	e	Classicals I ($N=28$)	−0.45	0.017	2.4
$R-I$	e	Classicals I ($N=26$)	0.02	0.91	0.1
$V-I$	e	Classicals I ($N=26$)	−0.32	0.11	1.6
$B-R$	e	Classicals I ($N=27$)	−0.43	0.026	2.2
$B-I$	e	Classicals I ($N=25$)	−0.36	0.076	1.8
$B-R$	a	Classicals I ($N=27$)	0.26	0.19	1.3
$B-V$	i	Classicals I ($N=27$)	−0.73	1.7e−05	4.3
$V-R$	i	Classicals I ($N=28$)	−0.3	0.12	1.6
$R-I$	i	Classicals I ($N=26$)	−0.38	0.057	1.9
$V-I$	i	Classicals I ($N=26$)	−0.44	0.025	2.2
$B-R$	i	Classicals I ($N=27$)	−0.65	0.0003	3.6
$B-I$	i	Classicals I ($N=25$)	−0.57	0.0029	3.0
$B-V$	$V-R$	Classicals II ($N=20$)	−0.00	0.99	0.0
$B-V$	$R-I$	Classicals II ($N=18$)	−0.28	0.25	1.1
$V-R$	$R-I$	Classicals II ($N=19$)	−0.31	0.20	1.3
$B-V$	q	Classicals II ($N=20$)	0.17	0.48	0.7
$V-R$	q	Classicals II ($N=21$)	0.28	0.21	1.2
$R-I$	q	Classicals II ($N=19$)	−0.37	0.12	1.6
$V-I$	q	Classicals II ($N=19$)	−0.03	0.89	0.1
$B-R$	q	Classicals II ($N=20$)	0.23	0.32	1.0
$B-I$	q	Classicals II ($N=18$)	0.12	0.63	0.5
$B-V$	e	Classicals II ($N=20$)	−0.02	0.93	0.1
$V-R$	e	Classicals II ($N=21$)	−0.21	0.37	0.9
$R-I$	e	Classicals II ($N=19$)	0.37	0.12	1.6
$V-I$	e	Classicals II ($N=19$)	0.11	0.65	0.5
$B-R$	e	Classicals II ($N=20$)	−0.08	0.74	0.3
$B-I$	e	Classicals II ($N=18$)	−0.01	0.96	0.0
$B-R$	a	Classicals II ($N=20$)	0.07	0.75	0.3
$B-V$	i	Classicals II ($N=20$)	−0.59	0.006	2.8
$V-R$	i	Classicals II ($N=21$)	0.19	0.41	0.8
$R-I$	i	Classicals II ($N=19$)	−0.02	0.93	0.1
$V-I$	i	Classicals II ($N=19$)	0.13	0.59	0.5
$B-R$	i	Classicals II ($N=20$)	−0.41	0.074	1.8
$B-I$	i	Classicals II ($N=18$)	−0.18	0.48	0.7
$B-V$	q	Hot Classicals I ($N=17$)	0.41	0.1	1.6
$V-R$	q	Hot Classicals I ($N=17$)	0.83	4.1e−05	4.1
$R-I$	q	Hot Classicals I ($N=15$)	0.17	0.54	0.6
$V-I$	q	Hot Classicals I ($N=15$)	0.63	0.012	2.5
$B-R$	q	Hot Classicals I ($N=17$)	0.7	0.0018	3.1
$B-I$	q	Hot Classicals I ($N=15$)	0.6	0.018	2.4
$B-V$	e	Hot Classicals I ($N=17$)	−0.16	0.53	0.6
$V-R$	e	Hot Classicals I ($N=17$)	−0.41	0.11	1.6
$R-I$	e	Hot Classicals I ($N=15$)	0.15	0.6	0.5
$V-I$	e	Hot Classicals I ($N=15$)	−0.2	0.47	0.7
$B-R$	e	Hot Classicals I ($N=17$)	−0.32	0.22	1.2
$B-I$	e	Hot Classicals I ($N=15$)	−0.16	0.57	0.6
$B-R$	a	Hot Classicals I ($N=17$)	0.42	0.09	1.7
$B-V$	i	Hot Classicals I ($N=17$)	−0.68	0.0027	3.0
$V-R$	i	Hot Classicals I ($N=17$)	−0.35	0.16	1.4
$R-I$	i	Hot Classicals I ($N=15$)	−0.34	0.22	1.2
$V-I$	i	Hot Classicals I ($N=15$)	−0.46	0.087	1.7

(*continued on next page*)

Table 6 (*continued*)

Quantity[a]	Quantity[a]	Group[b]	r_{corr}[c]	Prob[d]	SL[e]
$B-R$	i	Hot Classicals I ($N=17$)	−0.65	0.0047	2.8
$B-I$	i	Hot Classicals I ($N=15$)	−0.46	0.084	1.7
$B-R$	i	Hot Classicals II ($N=10$)	−0.59	0.07	1.8

[a] a = semi-major axis, e = eccentricity, i = inclination, q = perihelion.
[b] Dynamical class, according to Section 3, and number of measurements in the sample.
[c] Spearman's rank correlation statistic.
[d] Probability of obtaining a higher or equal coefficient of correlation from an uncorrelated set of data. $P < 0.003$ indicates a correlation with $> 3\sigma$ significance level (SL).
[e] Significance level (SL) of the correlation, derived from the probability and assuming Gaussian statistics. $P = 0.01$ means a 2.6σ significance. $P = 0.001$ confidence means a 3.3σ significance.

4.2. SDOs ($N = 10$ or 17)

We study SDO correlations considering two different possibilities for their classification, with subsequent changes in sample size (see Section 3 for classifications). For Classif. I ($N = 10$) the only reasonably strong evidence of a correlation is found for $B-V$ versus $R-I$ ($r = 0.69$, 2.2σ). For Classif. II ($N = 17$) we find similarly a strong correlation between $B-V$ and $R-I$ ($r = 0.68$, 3.0σ), while $B-V$ versus $V-R$ ($r = 0.49$, 2.0σ), and $V-R$ versus $R-I$ ($r = 0.50$, 2.0σ) show only evidence for a possible weak correlations. These results, different from the others EKB populations may suggest for several coloring agents instead of one. Peixinho et al. (2004) found reasonably strong mutual correlations for all the colors, but however with a smaller sample ($N = 13$) and below 3σ significance.

Like for Centaurs, the small sample size for the first classification scheme ($N = 10$) does not allow a reliable statistical work, and even for the second one ($N = 17$) risk factors of failing to detect strong correlations are larger than 20% ($\beta = 0.26$). On a sample twice as large as ours (taking the first classification hypothesis), Peixinho et al. (2004) did not find any meaningful trends with orbital parameters. However, they did note a clear lack of red surfaces among SDOs. This feature is obvious when looking at colored Figs. 1 and 2.

Clearly, further studies are needed not only by increasing sample size but also regarding their dynamical classification.

4.3. Plutinos ($N = 17$)

Looking at Figs. 1 and 2, it is visually clear that Plutino colors do not show any particular trends or evidence of correlations with any orbital parameters. This result does not change our previous finding that Plutinos appear to lack any evident trends in their surface colors. Only $B-V$ and $V-R$ colors are significantly correlated ($r = 0.65$, 2.8σ). Our sample does not show any color–absolute magnitude correlation, as seen by Hainaut and Delsanti (2002) and Peixinho et al. (2004).

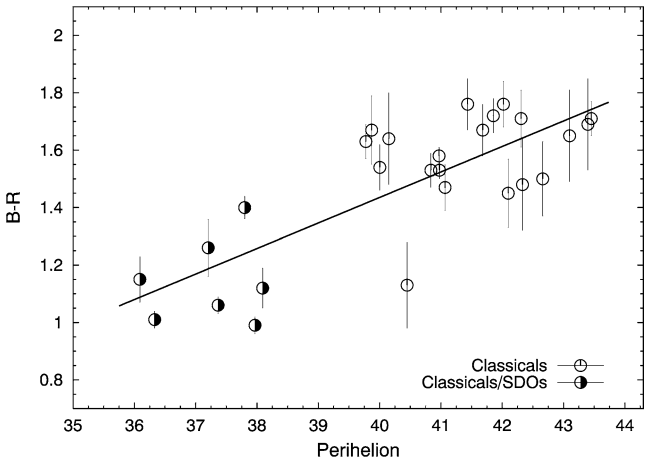

Fig. 3. $B-R$ color index versus perihelion distance plot for the Classical TNOs. Both the two different classifications (see text Section 3) for Classicals have been plotted. A linear least-squares fit has been plotted to illustrate the correlation.

4.4. Classicals ($N = 27$ or 20)

As for SDOs, we studied correlations among Classical objects considering two different possibilities for their classification (see Section 3 for classifications).

4.4.1. Classif. I ($N = 27$)

Under this classification scheme Classical objects show possible evidence for color–color correlations only between $B-V$ and $V-R$ ($r = 0.47$, 2.5σ).

Several color–orbital trends are exhibited. $B-V$ and $V-R$ show evidence for weak and strong correlations with perihelion distance (respectively $r = 0.52$, 2.8σ, and $r = 0.67$, 3.9σ), while $R-I$ shows no evidence for this trend. $B-R$, $V-I$, and $B-I$ are still correlated with q ($r = 0.65$, 3.7σ, $r = 0.55$, 2.9σ, and $r = 0.61$, 3.2σ). The $V-R$ seems to dominate this correlation. As to the color–orbital inclination correlations, $B-V$, $B-R$, and $B-I$ are all strongly correlated with inclination (respectively $r = -0.73$, 4.3σ, $r = -0.65$, 3.6σ, and $r = -0.57$, 3.0σ). In this case it is the $B-V$ color that dominates the correlation, as $V-R$ and $R-I$ do not show it. For $V-I$, the coefficient is rather weak. Stephens et al. (2003) who did not find any significant trend between $V-I$ and inclination had already suggested that this trend could be only present when including B magnitude information.

As in DOR02, we confirmed the strong and significant correlations ($r > 0.6$ and SL $> 3\sigma$) for $B-R$ color with inclination and with perihelion (Fig. 3). On the other hand, we find a weaker, and less evident correlation between $B-R$ color and eccentricity ($r = -0.43$, SL $= 2.2\sigma$) compared to the DOR02's result ($r = -0.60$, SL $= 3.5\sigma$).

4.4.2. Classif. II ($N = 20$)

Under this classification scheme our Classical objects are essentially a red group, quite clustered in semi-major axis and perihelion values (see Fig. 1). However, they do not

cluster significantly in inclination (see Fig. 2) and may be subdivided in 10 dynamically cold and 10 dynamically hot objects ($i = 4.5°$ limit). Only $B-V$ exhibits strong evidence for correlation with inclination ($r = -0.59$, 2.7σ), while other colors do not show this kind of evidence. There is no evidence for any other correlations, including color–color correlations. Additionally, with this classification scheme, we no longer detect the color–inclination correlation among the hot Classicals.

4.4.3. Hot Classicals

Tegler and Romanishin (2000) found that all TNOs in near-circular orbits beyond 40 AU have very red colors and should constitute a separate group. Other authors considered that two separate groups exist in function of orbital inclination (Levison and Stern, 2001; Brown, 2001). DOR02 and especially Peixinho et al. (2004), on a much larger dataset than this work, showed that, based on their color–inclination properties, Classicals (Classif. I scheme) seem to be made of two distinct populations: the red population which is a red cluster of dynamically cold TNOs, at $i < 4.5°$, and a dynamically hot population ($i > 4.5°$), both revealing very different color dispersions. A quick inspection of Fig. 2 makes this remarkable trend very convincing. However under the Classif. I scheme, we still find the same color–inclination and color–perihelion correlations for the dynamically hot population taken alone ($N = 17$) as we find for Classical TNOs as a whole (see Table 6). We find also that one object belonging to the "red cluster" has an unexpected neutral color ($B - R = 1.14$, this object clearly detached from Fig. 2). This object, 2001 QY_{297}, also shows some color variation (see Section 3.3). Obviously, this object needs to be re-observed to confirm and get more accurate colors.

4.5. Resonance 5:2 ($N = 4$)

There are four objects located in the 5:2 resonance: 1999 DE_9, 1999 HB_{12}, 2000 FE_8, and 2002 GP_{32} (Chiang et al., 2003a, 2003b). Colors of these objects appear similar with a value around $B - R = 1.3$–1.5.

5. Comparisons with associated populations

It has been thought that many small body populations are related through a common origin in the EKB. These include the short period comets, dead comets, Centaurs, and irregular satellites (see Jewitt, 2002).

5.1. The short period comets

The short period comet (SPC) connection with TNOs appears the strongest and oldest link with the EKB. This establishment was demonstrated by Fernández (1980) to explain the flux of the near ecliptic comets. However no consensus exists on which part of the EKB the SPCs are derived from. Among the suspected TNO families the SDOs may constitute a dominant source (Duncan and Levison, 1997), thanks to their perihelic interaction with Neptune. The giant planet may have progressively scattered out SDOs into their present orbits on timescales of order 1 Gyr. Another plausible source for SPCs are the Plutinos (Yu and Tremaine, 1999). In that case collisional fragments ejected in the chaotic zones at the boundaries of resonances would be scattered by Pluto. Comparing the physical data, e.g., colors would be very meaningful in learning how linked is this likely related population. Such interesting questions include "which part of the EKB might be the dominant reservoir of SPCs." To this purpose we used the latest dataset of cometary nuclei of SPCs compiled by Lamy et al. (2005).

The Kruskal–Wallis test (Kruskal and Wallis, 1952) computes the probability (i.e., the significance level) that two populations are extracted from the same parent population. A zero probability means that the two populations are different (technically: with different mean values) while a unit probability means they appear to be identical. This test is somewhat comparable to another non-parametric test, the Kolmogorov–Smirnov, but has the advantage of analyzing several distributions in one single test. We thus compared the $V - R$ color distribution of all six families, including their different classification schemes (Centaurs, comets, SDOs I, SDOs II, Classical objects I, Classical objects II, Plutinos and irregular satellites). Considering the $V - R$ instead of $B - R$ color permitted us to have a significantly larger sample of SPC data ($N = 20$).

We found that the probability of Classicals (both Classif. I and II) and comets being drawn from the same single parent population is $P < 4 \times 10^{-5}$. The two populations are thus incompatible at a highly significant level of SL $> 4.1\sigma$. We also found significant incompatibility results for the Plutinos (SL $= 3.2\sigma$) and the Centaurs (SL $= 2.6\sigma$). On the other hand, we found that comets and SDOs (both Classif. I and II) could be drawn from a same single parent distribution ($P > 0.159$, SL $< 1.4\sigma$, therefore smaller than the minimum 2σ to show reasonable evidence for incompatibility).

Figure 4 shows the color–color plot of TNOs, Centaurs, comets and irregular satellites. The cometary nuclei appear bluer than the Centaurs or any EKB dynamical group. In other words, cometary nuclei lack the very red color ($B - V > 0.9$, $V - R > 0.6$) that is common among TNOs and Centaurs. This result has been pointed out by Doressoundiram et al. (2001) and further investigated by Jewitt (2002). Surprisingly, results show that colors of cometary nuclei do not match simultaneously their TNO and Centaur precursors, and thus suggest that some process modifies the surface of SPCs after entering into the inner Solar System. Jewitt (2002) suggested active comets have been resurfaced either by the accumulation of Classical lag deposits or by fallback of sub-orbital debris. The timescale for mantling has been estimated from simple models and is found to be very short inside the orbit of Jupiter (e.g., 10^3 yrs at 3 AU, Jewitt, 2002). Therefore, the very red material,

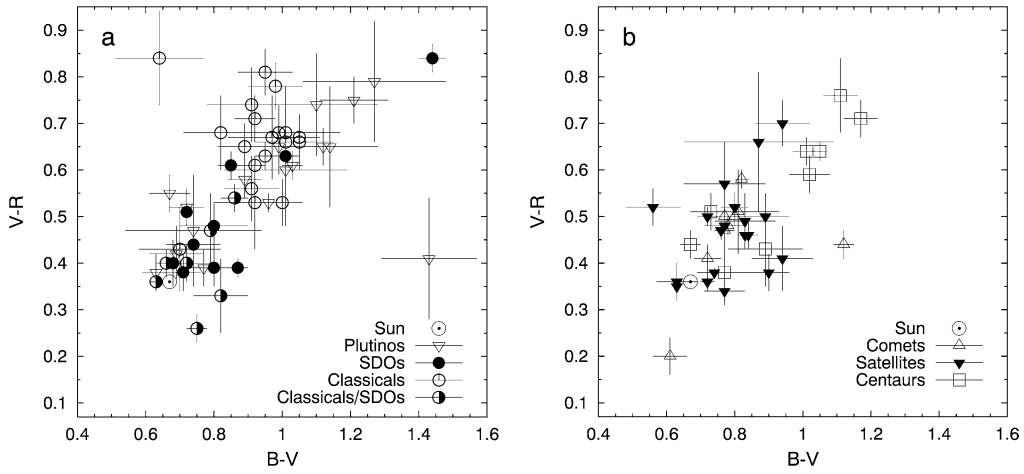

Fig. 4. $B-V$ versus $V-R$ color plots of TNOs, Centaurs, cometary nuclei and irregular satellites. The two different classifications (see text Section 3) for Classicals and SDOs have been plotted. The dotted circle represents colors of the Sun.

probably of highly polymerized organic matter formed in the Kuiper belt after eons of prolonged irradiation, does not survive entry in the inner Solar System. However, it could still exist underneath.

5.2. The Centaurs

The Centaurs are a dynamical family of objects on chaotic orbits whose semi-major axes fall between those of Jupiter and Neptune, with a dynamical lifetime measured in millions of years (Hahn and Bailey, 1990). Long-term orbital integrations of the TNOs suggest that perturbations by the giant planets provide a source of Centaurs and short period comets (Duncan and Levison, 1997). About 60 Centaurs have been identified among the 1000 TNOs and Centaurs known to date (September, 2004). They have very eccentric orbits, with perihelia between 5 and 30 AU. As shown by the previous color surveys (see Doressoundiram, 2003) the range of colors for both TNOs and Centaurs is very large, from neutral to very red. Centaurs and trans-neptunian objects may therefore be part of a same class of objects. Now that we have enough color data in individual EKB dynamical classes, we raise the question which part of the EKB the Centaurs may have been derived from. This problem is indeed connected to the origin of SPCs discussed in the previous section.

Not surprisingly, the Kruskal–Wallis (KW) test[2] validates the compatibility of Centaurs with TNOs as a whole ($P = 0.839$, i.e., $P \gg 0.05$ or SL $\ll 2\sigma$ boundary values for reasonable evidence of incompatibility). However, the KW test also assesses the compatibility of Centaurs with each of the EKB dynamical groups. This result does not allow identifying a privileged source region of the EKB based on color properties alone. Nonetheless, we should mention that the probability that Plutinos and Centaurs were drawn from the same parent distribution is $P = 0.964$ a much higher value than those obtained for other populations (0.237 for SDOs I, and 0.509 for Classicals I), while there is reasonably strong evidence that they are incompatible with SDOs II ($P = 0.037$, SL $= 2.1\sigma$). Peixinho et al. (2004), considering only SDOs I, reached the same conclusion based on the analysis of the color–color correlations. They found for a dataset of 109 objects that Centaur' color–color correlations were very similar with those of Plutinos.

In Fig. 4 it is noteworthy that the color distribution of Centaurs is clearly bimodal with one group having neutral/slightly red color and the other very red colors. This finding was recently statistically assessed by Peixinho et al. (2003). For the first time, they separately analyzed Centaurs and TNO populations and clearly demonstrated that the Centaurs' color distribution is bimodal while the TNOs' color distribution, as a whole, is definitively unimodal.

This color dichotomy is further enhanced by the fact that Chiron (which belongs to the neutral group) is recognized as an active comet, which is not the case of Pholus (which belongs to the very red group). The extremely red colors of Pholus may represent a more pristine surface while the neutral/slightly red color of Chiron may be due to outgassing during successive perihelion passages. This may indicate that a thick enough irradiation-mantle may have formed on the surface of Pholus which inhibits outgassing of volatiles, whereas Chiron exhibits a less red, more neutral surface reworked by cometary activity. Therefore, it is tempting to conclude, as also suggested by Luu et al. (2000), that the "Chiron group" (Hylonome, Asbolus, ...) have or had cometary activity that removed or covered their eventual irradiation mantle while the "Pholus group" (Nessus, 1999 OX_3, ...) are those objects which did not experience cometary activity or impact cratering.

Resurfacing processes responsible for the removal of the reddish crust among the TNO population should be dominated by impact cratering (Durda and Stern, 2000), with cometary outbursts being marginal. On the other hand, it should be the opposite case among the Centaurs since

[2] In the two-sample case the test is called Mann–Whitney.

they get closer to the Sun while experiencing fewer collisions (they occupy regions less densely populated than the Edgeworth–Kuiper belt). Therefore, since Centaurs are presumably escapees from the EKB, only those with the reddest colors (i.e., global thick reddish crust) may resist solar heating of the surface and keep their irradiation mantle. On the other hand, those with neutral/slightly red (freshly impact reworked surfaces) will easily sublimate their super volatiles (e.g., CO, N_2). What about the lack of Centaurs with intermediate colors (escaped TNOs with intermediate colors)? We suggest that those missing Centaurs (reddish crust with patches of excavated craters) will have cometary activity triggered by their exposed areas, which in turn will process the entire surface, making the global colors more neutral. This "blue-shift" of originally intermediate objects may be responsible for the actual bimodality in the Centaurs.

5.3. The irregular satellites

While the so-called regular satellites have nearly circular and low-inclination orbits, the irregular satellites follow eccentric, highly inclined, and often-retrograde orbits. Like Centaurs and short period comets, irregular satellites are probably escaped objects from the Edgeworth–Kuiper belt subsequently captured by the giant planets. For this reason, these objects are of considerable interest for comparison of their dynamical, physical and chemical properties which may give insights on their origin as well as the history and evolution of the trans-neptunian objects.

For the purpose of our analysis, we collected the *BVR* photometry of irregular satellites ($N = 26$) from Grav et al. (2003), Rettig et al. (2001), Maris et al. (2001), Romon et al. (2001) and Schaefer and Schaefer (2000).

According to the KW test, the $V - R$ color distribution of irregular satellites is different from those of Centaurs, Plutinos, and Classical TNOs. The incompatibilities obtained are significant ($P = 0.023$, SL $= 2.3\sigma$ for Centaurs; $P = 0.004$, SL $= 2.9\sigma$ for Plutinos; $P < 4 \times 10^{-5}$, SL $> 4.1\sigma$, both for Classicals I and II) demonstrating that the irregular satellite population is not compatible with any of the Centaur, Plutino or Classical populations. Grav et al. (2003) also found that *BVRI* colors of irregular satellites lack the red to very red colors of Centaurs and TNOs.

On the other hand, we find that irregular satellites and SDOs (both Classif. I and II) could be extracted from the same parent population ($P = 0.37$, SL $= 0.9\sigma$ for SDOs I; and $P = 0.97$, SL $< 0.1\sigma$ for SDOs II), that is, the color properties of satellites and SDOs are comparable. This result is not surprising since SDOs have, globally, a bluer color distribution. Therefore, on a color basis, SDOs could be the source of irregular satellites. However, this last result should be taken with caution because (1) the statistics of SDOs is very low ($N = 10$, in the worst case), (2) even though we considered two possible classification schemes, there are no strict dynamical definition of Classicals and SDOs and the dynamical stability of several members of each class is not well assessed.

6. Summary

In recent years, the broadband colors on trans-neptunian objects (TNOs) have greatly increased the knowledge of their surface properties. With the large and high quality color datasets available, strong and significant results have been found. We present here the latest $B - V$, $V - R$, and $R - I$ color measurements obtained with the CFH12K mosaic camera on the 3.6-m Canada–France–Hawaii Telescope (CFHT). This work is the latest extension of the Meudon Multicolor Survey (2MS), a dataset that now totals 71 Centaurs and TNOs. In previous work (Doressoundiram et al., 2002), we found significant correlations between some optical colors and some orbital parameters (e.g., perihelion) for the classical Kuiper belt. On the other hand, no unequivocal color–orbital trends were obvious for Plutinos, scattered objects or Centaurs. In this new and larger dataset of 71 objects we confirm all the correlations previously found except the color–eccentricity correlation for Classical TNOs.

We also make for the first time reliable statistical comparison between TNOs and related populations (e.g., Centaurs, irregular satellites, cometary nuclei). Our results show that (1) colors of cometary nuclei do not match both their TNO and Centaur precursors, and this suggests that some process modifies the surface of SPCs at entry into the inner Solar System. The only exception concerns colors of SDOs from which we could statistically assess that comets and SDOs could be drawn from the same single parent distribution. (2) Though Centaurs are compatible with most of the EKB dynamical groups at a highly significant level (Plutino being the most similar population), surprisingly, they hint for incompatibility with SDOs. (3) Centaur colors still present a strong dichotomy between a neutral/slightly red group (e.g., Chiron) and a very red group (e.g., Pholus). This is probably related to cometary activity, which reworked and refreshed the surface in the case of Chiron but was inhibited by a red, thick, crust in the case of Pholus. Cometary activity is also responsible for the lack of Centaurs with intermediate colors. Indeed, if we suppose that intermediate colors are due to partially cratered objects (reddish crust with patches of excavated craters) then cometary activity will be triggered by the exposed areas. This "blue-shift" of originally intermediate objects may be responsible for the observed bimodality in the Centaurs. The colors of cometary nuclei similar to the "Chiron" group seem to confirm that neutral/slightly red color is diagnostic of cometary activity. (4) The irregular satellite population is not compatible with any of the Centaur, Plutino or Classical populations. Nonetheless, we found that irregular satellites and SDOs can be extracted from the same parent population, since color properties of satellites and SDOs are comparable. However, results for Centaurs

and SDOs should be taken with care, as usual when dealing with small numbers.

Acknowledgments

This work was made possible by support of the French "Programme National de Planétologie." We thank CFHT Time Allocation Committee for consistent allocation of telescope time. The Canada–France–Hawaii Telescope (CFHT) is operated by the National Research Council of Canada, the Centre National de la recherche Scientifique of France and the University of Hawaii. We are very grateful to anonymous referees who did a wonderful job giving helpful comments and suggestions. N.P. acknowledges funding from the Portuguese Foundation for Science and for Technology (ref: SFRH/BD/1094/2000).

References

Barucci, M.A., Doressoundiram, A., Fulchignoni, M., Tholen, D., Lazzarin, M., 1999. Spectrophotometric observations of Edgeworth–Kuiper belt objects. Icarus 142, 476–481.

Barucci, M.A., Romon, J., Doressoundiram, A., Tholen, D., 2000. Compositional surface diversity in the trans-neptunian objects. Astron. J. 120, 496–500.

Bauer, J.M., Meech, K.J., Fernández, Y.R., Farnham, T.L., Roush, T.L., 2002. Observations of the Centaur 1999 UG_5: evidence of a unique outer Solar System surface. Publ. Astron. Soc. Pacific 114, 1309–1321.

Bauer, J.M., Fernández, Y.R., Meech, K.J., 2003a. An optical survey of the active Centaur C/NEAT (2001 T4). Publ. Astron. Soc. Pacific 115, 981–982.

Bauer, J.M., Meech, K.J., Fernández, Y.R., Pittichova, J., Hainaut, O.R., Boehnhardt, H., Delsanti, A.C., 2003b. Physical survey of 24 Centaurs with visible photometry. Icarus 166, 195–211.

Belskaya, I.N., Barucci, M.A., Shkuratov, Y.G., 2003. Opposition effect of KBOs, preliminary estimations. Earth Moon Planets 92, 201–206.

Boehnhardt, H., Tozzi, G.P., Birkle, K., Hainaut, O., Sekiguchi, T., Vlair, M., Watanabe, J., Rupprech, G., the Fors Instrument Team, 2001. Visible and near-IR observations of trans-neptunian objects. Results from ESO and Calar Alto telescopes. Astron. Astrophys. 378, 653–667.

Brown, M.E., 2001. The inclination distribution of the Kuiper belt. Astron. J. 121, 2804–2814.

Brown, M.E., Trujillo, C.A., 2004. Direct measurement of the size of the large Kuiper belt object (50000) Quaoar. Astron. J. 127, 2413–2417.

Chiang, E.I., Jordan, A.B., Millis, R.L., Buie, M.W., Wasserman, L.H., Elliot, J.L., Kern, S.D., Trilling, D.E., Meech, K.J., Wagner, R.M., 2003a. Resonance occupation in the Kuiper belt: case examples of the 5:2 and Trojan resonances. Astron. J. 126, 430–443.

Chiang, E.I., Lovering, J.R., Millis, R.L., Buie, M.W., Wasserman, L.H., Meech, K.J., 2003b. Resonant and secular families of the Kuiper belt. Earth Moon Planets 92, 49–62.

Delsanti, A., Hainaut, E., Jourdeuil, E., Meech, K.J., Boehnhardt, H., Barrera, L., 2004. Simultaneous visible-near IR photometric study of Kuiper belt objects surfaces with ESO/Very Large Telescopes. Astron. Astrophys. 417, 1145–1158.

Doressoundiram, A., 2003. Colour properties and trends in trans-neptunian objects. Earth Moon Planets 92, 131–144.

Doressoundiram, A., Boehnhardt, H., 2003. Multicolour photometry of trans-neptunian objects: surface properties and structures. C. R. Acad. Sci. Paris 4, 755–765.

Doressoundiram, A., Barucci, M.A., Romon, J., Veillet, C., 2001. Multicolor photometry of trans-neptunian objects. Icarus 154, 277–286.

Doressoundiram, A., Peixinho, N., De Bergh, C., Fornasier, S., Thebault, Ph., Barucci, M.A., Veillet, C., 2002. The color distribution of the Kuiper belt. Astron. J. 124, 2279–2296.

Duncan, M., Levison, H., 1997. A scattered comet disk and the origin of Jupiter family comets. Science 276, 1670–1672.

Duncan, M.J., Levison, H.F., Budd, S.M., 1995. The dynamical structure of the Kuiper belt. Astron. J. 110, 3073–3190.

Durda, D.D., Stern, S.A., 2000. Collision rates in the present-day Kuiper belt and Centaurs regions: application to surface activation and modification on comets, Kuiper belt objects, Centaurs, and Pluto–Charon. Icarus 145, 220–229.

Fernández, J.A., 1980. On the existence of a comet belt beyond Neptune. Mon. Not. R. Astron. Soc. 192, 481–491.

Grav, T., Holman, M.J., Gladman, B., Aksnes, K., 2003. Photometric survey of the irregular satellites. Icarus 166, 33–45.

Hahn, Bailey, 1990. Rapid dynamical evolution of giant Comet Chiron. Nature 348, 132–136.

Hainaut, O.R., Delsanti, A.C., 2002. Colors of minor bodies in the outer Solar System. Astron. Astrophys. 389, 641–664.

Howell, S.B., 1989. Two-dimensional aperture photometry. Signal-to-noise ratio of point-source observations and optimal data-extraction techniques. Publ. Astron. Soc. Pacific 101, 616–622.

Jewitt, D., 2002. From Kuiper belt object to cometary nucleus: the missing ultra-red matter. Astron. J. 123, 1039–1049.

Jewitt, D., Luu, J.X., 2001. Colors and spectra of Kuiper belt objects. Astron. J. 122, 2099–2114.

Kruskal, W.H., Wallis, W.A., 1952. Use of ranks on one-criterion variance analysis. J. Am. Stat. Assoc. 47, 538–621.

Kuchner, M.J., Brown, M.E., Holman, M., 2002. Long-term dynamics and the orbital inclinations of the classical Kuiper belt objects. Astron. J. 124, 1221–1230.

Landolt, A., 1992. UBVRI photometric standard stars in the magnitude range 11.5–16.0 around the celestial equator. Astron. J. 104, 340–371.

Lamy, P.L., Toth, I., Fernández, Y.R., Weaver, H.A., 2005. The sizes, shapes, albedos, and colors of cometary nuclei. In: Festou, M., Keller, H.U., Weaver, H.A. (Eds.), Comets II. Univ. of Arizona Press, Tucson. In press.

Levison, H.F., Stern, S.A., 2001. On the size dependence of the inclination distribution of the main Kuiper belt. Astron. J. 121, 1730–1735.

Luu, J.X., Jewitt, D., 1996. Color diversity among the Centaurs and Kuiper belt objects. Astron. J. 112, 2310–2318.

Luu, J.X., Jewitt, D.C., Trujillo, C., 2000. Water ice in 2060 Chiron and its implications for Centaurs and Kuiper belt objects. Astrophys. J. 531, L151–L154.

Maris, M., Carraro, G., Cremonese, G., Fulle, M., 2001. Multicolor photometry of the Uranus irregular satellites Sycorax and Caliban. Astron. J. 121, 2800–2803.

McBride, N., Green, S.F., Hainaut, O., Delahodde, C., 1999. The "MBOSS data reduction consortium," Kuiper belt photometry: getting the best you're your observations, asteroids, comets, meteors, Cornell University, July 26–30, 1999, USA.

McBride, N., Green, S.F., Davies, J.K., Tholen, D.J., Sheppard, S.S., Whiteley, R.J., Hillier, J.K., 2003. Visible and infrared photometry of Kuiper belt objects: searching for evidence of trends. Icarus 161, 501–510.

Peixinho, N., Doressoundiram, A., Delsanti, A., Boehnhardt, H., Barucci, M.A., Belskaya, I., 2003. Reopening the TNOs color controversy: Centaurs bimodality and TNOs unimodality. Astron. Astrophys. 410, L29–L32.

Peixinho, N., Boehnhardt, H., Belskaya, I., Doressoundiram, A., Barucci, M.A., Delsanti, A., 2004. ESO Large Program on Centaurs and TNOs: final results. Icarus 170, 153–166.

Rettig, T.W., Walsh, K., Consolmagno, G., 2001. Implied evolutionary differences of the jovian irregular satellites from a BVR color survey. Icarus 154, 313–320.

Romon, J., De Bergh, C., Barucci, M.A., Doressoundiram, A., Cuby, J.-G., Le Bras, A., Douté, S., Schmitt, B., 2001. Photometric and spectroscopic observations of Sycorax, satellite of Uranus. Astron. Astrophys. 376, 310–315.

Schaefer, B.E., Schaefer, M.W., 2000. Nereid has complex large-amplitude photometric variability. Icarus 146, 541–555.

Sheppard, S.S., Jewitt, D.C., 2002. Time-resolved photometry of Kuiper belt objects: rotations, shapes, and phase functions. Astron. J. 124, 1757–1775.

Spearman, C., 1904. The proof and measurement of association between two things. Am. J. Psychol. 57, 72–101.

Stephens, D.C., Noll, K.S., Grundy, W.M., Millis, R.L., Spencer, J.R., Buie, M.W., Tegler, S.C., Romanishin, W., Cruikshank, D.P., 2003. HST photometry of trans-neptunian objects. Earth Moon Planets 92, 251–260.

Tegler, S.C., Romanishin, W., 2000. Extremely red Kuiper-belt objects in near-circular orbits beyond 40 AU. Nature 407, 979–981.

Tegler, S.C., Romanishin, W., Consolmagno, S.J., 2003. Color patterns in the Kuiper belt: a possible primordial origin. Astrophys. J. 599, L49–L52.

Torbett, M.V., Smoluchowski, R., 1990. Chaotic motion in a primordial comet disk beyond Neptune and comet influx to the Solar System. Nature 345, 49–51.

Trujillo, C.A., Brown, M.E., 2002. A correlation between inclination and color in the classical Kuiper belt. Astrophys. J. 566, L125–L128.

Yu, Q., Tremaine, S., 1999. The dynamics of Plutinos. Astron. J. 118, 1873–1881.